Verdú Amat, S.; Pérez Jiménez, AJ.; Barat Baviera, JM.; Grau Meló, R. (2019). Laser backscattering imaging as a control technique for fluid foods: Application to vegetable-based creams processing. Journal of Food Engineering. 241:58-66. https://doi.org/10.1016/j.jfoodeng.2018.08.003

Laser backscattering imaging as a control technique for fluid foods: Application to vegetable-based creams processing

Samuel Verdú[a,*], Alberto J. Pérez[b], José M. Barat[a], Raúl Grau[a]

[a] Departamento de Tecnología de Alimentos, Universidad Politècnica de València, Spain
[b] Departamento de Informática de Sistemas y Computadores, Universidad Politècnica de València, Spain

ARTICLE INFO

Keywords:
Vegetable cream
Imaging analysis
Laser backscattering
Rheology
Quality control

ABSTRACT

In this work, the application of a laser backscattering image technique as a non-destructive quality control technique for fluid food matrices was studied. The used food matrices were vegetable-based creams, which were modified according to the combination of four production factors (raw material, biopolymer type, biopolymer concentration and homogenisation system) in order to obtain a wide space of variance in terms of physico-chemical properties (52 different creams). All the creams were characterised based on that imaging technique using pre-designed descriptors extracted from the captures of the generated laser patterns. The capacity to characterise creams presented by the imaging and physico-chemical data (rheology and syneresis) was compared, and the effect of each production factor on their captured variance was evaluated. Both characterisations were similar. This parallelism was proved by modelling the relationship between them by carrying out regression studies. The regression coefficients were successful for most physico-chemical variables. However, the prediction of creams' properties was maximised when done over the linear combination of them all. Thus the imaging descriptors collected enough variance from the cream categories to place them according to their physico-chemical properties into the generated space of physico-chemical variance. The results allowed us to conclude that this technique can be applied for the non-destructive quality control of fluid-food matrices for production processes with a wide spectrum of product categories.

1. Introduction

The continuous improvement of processing control in the food industry is based on motivation, which affects both the most traditional and the newest quality and safety processes. The main improvement areas focus on reducing operation times, energy costs and waste. These improvements in control and inspection on production lines can be generally made by substituting outdated equipment and technologies, modifying equipment materials, etc. Indeed modifying and adapting new techniques to the analysis and control procedures in production processes can lead to major short-term improvements without them implying high economic and time costs (Abdul Halim Lim, Antony, Garza-Reyes and Arshed, 2015; Lim and Antony, 2016). One of the most important tendencies of this approach is to implement techniques that quickly collect vast amounts of data from process chain operations. The collected data can be used as a basis to generate a database of the entire production plant features for information about all processes, operations and products to be represented on a plausible map. From this map, knowledge about the entire activity can increase given the possibility of using automatic learning applications to then improve decision making about any modifications required at any time.

The tendency for developing devices and techniques for this purpose is being operating non-destructively. This implies using some physico-chemical principle to collect data without coming into contact with, or modifying, samples. In the food industry, this research area represents not only optimising resources for processing, but also major advances in quality/safety control terms that range from raw material reception to end product storage given the reduction of plausible contamination points (Arendse et al., 2018).

Some of the techniques are based on spectroscopic determinations (Barbin et al., 2015), ultrasounds (de Prados et al., 2015), electronic tongues (Fuentes et al., 2017), image analyses (Verdú et al., 2017), and some combinations of them all. The physico-chemical nature of the food matrix, as well as the specific transformations that take place during a given operation, restrict the suitability of each technique to measure a given analyte and then condition the requirements of applications. In

line with this, laser light backscattering image techniques match this purpose since food matrices are frequently semi-transparent or opaque, and thus allow light to pass at specific wavelengths (Mireei et al., 2010). It has been used successfully to control and model fruit inspection, classification and drying processes, and to determine moisture and solutes of some vegetables. Mollazade et al. (2012) and Adebayo et al. (2016) reported important compilations about applications of this technique in agro-food products. Meat processing has also been modelling in terms of water content and proteolysis, concretely for dry cured ham (Fulladosa et al., 2017).

These applications share the feature that they have been applied to a solid matrix to determine variables that imply important physico-morphological changes. Nevertheless, studies into fluid foods where subtle variations happen are lacking. This is a large field of applications since other light scattering-based techniques are already used to analyse this type of food matrix in laboratory assays. Some measure the droplet size distributions of emulsions by the laser diffraction technique, or take multiple light scattering measurements according to ageing time to estimate their physical stability.

There are numerous types of fluid-matrix foods; e.g. smoothies, vegetable creams, soups, spreadable, dairy, etc., which texture represents the main quality attribute of products. In that sense, these products are usually provided homogeneous in terms of texture; however, some factors could modify this property. These factors could be: changes in the origins of raw material, fats reduction, fibre increasing, etc. That modification could be a problem for certain type of consumer. For some fluid foods, the exhaustive control of texture represents not only organoleptic acceptance, but also one of the most important safety features of products. One relevant example of this is texture-modified foods for the elderly, which have a group of products with these characteristics, specifically the categories from “thin drinks” to “pureed” (from 50 to 1750 cP) according to the IDDS (*International dysphagia diet standardization initiative*). Therefore, rapidly increasing knowledge about the range of products generated in a production process could improve the quality and safety assurance possibilities of the last-hour changes produced because above mentioned modifications due to external causes.

Following this idea, the aim of this work was to study the effects of several production factors on the capability of laser light backscattering imaging to characterise the physico-chemical properties of vegetable-based creams.

2. Material and methods

2.1. Experiment procedure

The experiment aims to model a defined space of vegetable-based cream categories in terms of physico-chemical properties using a computer vision system and machine-learning procedures (Fig. 1). The objective of this procedure was to collect information non-destructively about all the cream categories produced on a plausible production plant to improve quality control once the product is finished. The first phase was the production of all the cream categories by combining four factors: F1 = raw material, F2 = biopolymer type, F3 = biopolymer concentration and F4 = homogenisation system. Factors were combined at different levels and into sub-categories to generate an extended space of variance for the physico-chemical properties from a many different products: fifty-two cream categories (Fig. 1–1). The second phase involved the characterisation of all the cream categories by means of physico-chemical analytics (rheology and syneresis procedures) and imaging analyses (previously developed image descriptors) (Figs. 1–2). Then two data blocks (physico-chemical and imaging descriptors) were obtained from each cream category in parallel. The third experiment phase involved exploring both data blocks to analyse the variance generated due to the effect of the factors combination (Figs. 1–3), and to thus evaluate the capacity of the imaging descriptors obtained to collect it. The last phase was to analyse both data blocks jointly to study the correlation between them (Figs. 1–4). In this phase, the regression coefficients were evaluated to obtain models to predict the physico-chemical features of all the cream categories in the generated variance space using the image features information.

2.2. Raw materials

All the cream categories were produced based on four main formulae. These formulae were produced according to a common base of ingredients, where the specific ingredient of each formula varied between two different vegetables or two different animal tissues. The common ingredient base contained 63% water, 10% carrot, 7% potato, 4% tomato, 3.5% red pepper, 2.5% onion, 1.5% extra olive oil and 0.7% salt (w.b). The remaining 10% was completed with the specific ingredients of each main formula: zucchini, spinach, fish (hake) or chicken (breast) (Fig. 1). All the ingredients were acquired as fresh products in local distributors.

2.3. Creams processing

The amount of processed cream was 1 kg/category in triplicate. All the cream categories were prepared according to the following phases:

1. Preparing raw material: operations to peel, wash and remove undesired parts manually (bones, thorns, skin, crusts, etc.)
2. Reducing particle size: products were cut with a cooking robot (Thermomix®, Worwerk) into a small particle size ($\leq$10 mm) to increase the surface.
3. Mixing and cooking: the cut products were mixed with water and boiled for 1 h.
4. Blending: After boiling time, the mix of products was blended for 5 min at 300 rpm in a cooking robot (Thermomix®, Worwerk).
5. Homogenisation: this phase was applied only to the modified creams. Biopolymers were added and homogenised with one of these three different systems (Fig. 1) for 3 min at 500 rpm:
   - Cooking robot (Thermomix®, Worwerk)
   - Industrial mixer (Neptune Gear Drive Mixer JG-2.0)
   - Homogenizer (IKA® Ultra-Turrax® T25 Digital Homogenizer)
6. Packing: creams were packaged at 65 °C in 250-mL glass jars with a twist-off closing system.
7. Sterilization: the packaged creams were heat-treated in an autoclave (Rodwell Ensign) at 121 °C/15 min/2.2 Bar.

2.4. Physico-chemical characterisation of creams

2.4.1. Rheological analysis

The rheological characterisation of creams was carried out by analysing flux behaviour in a rotational rheometer (Haake Rheostress 1, Thermo Electric Corporation, Karlsruhe, Germany) with a type Z34DIN Ti sensor system of coaxial cylinders. Shear stress (σ) was measured according to the shear rate (γ) from 0 to 200 s^{-1} and from 200 to 0 s^{-1}. Maximum shear stress was maintained for 2 min between both sweeps to determine tixotropy by calculating the hysteresis area (H). The obtained curves were modelled using Oswald's power law, from which the consistence index (K) and flux behaviour index (n) were deduced (Equation (1)). The apparent viscosity values were calculated at 100 s^{-1} for both curves.

$$\sigma = K\gamma^{n} \quad (1)$$

Finally, seven rheological features were used for each cream: the consistence index (K), the flux behaviour index (n) and apparent viscosity (η) from the first sweep, the same from the second sweep (K', n' and η'), and the hysteresis area (H). The analysis was done in triplicate for each cream category.

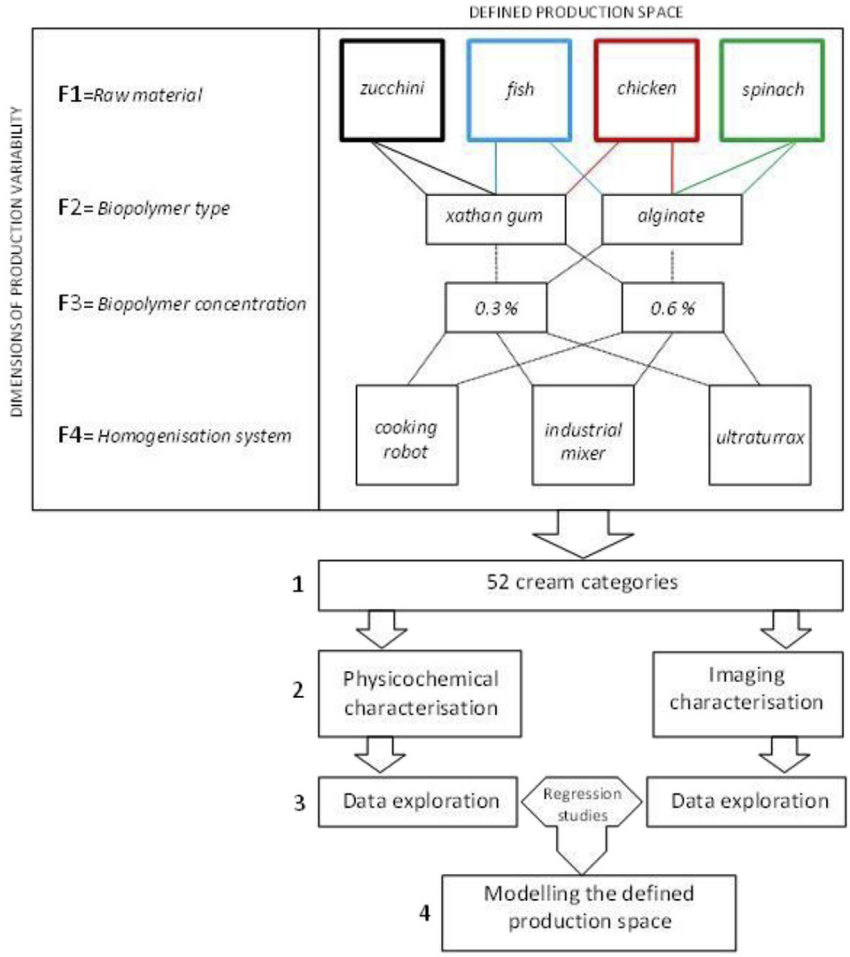

Fig. 1. Scheme of experimental procedure. Defined space of physicochemical variance by combining cream production factors. Numbers mean the order for activities.

2.4.2. Syneresis

The generated variability of the cream matrix's capacity to maintain the liquid phase of the product was tested by analysing syneresis (Mizrahi, 2010). This analysis was done by centrifuging 30 g of cream at 14,500 rpm/30 min. After this phase, the supernatant was collected and weighed. The analysis was done in triplicate for each cream category. The result was expressed as a percentage of syneresis (S_y), which was calculated based on Equation (2):

$$Sy = \frac{g\ supernatant}{g\ of\ cream} * 100 \quad (2)$$

2.4.3. Proximal composition

Proximal composition was analysed to know the effect of the raw

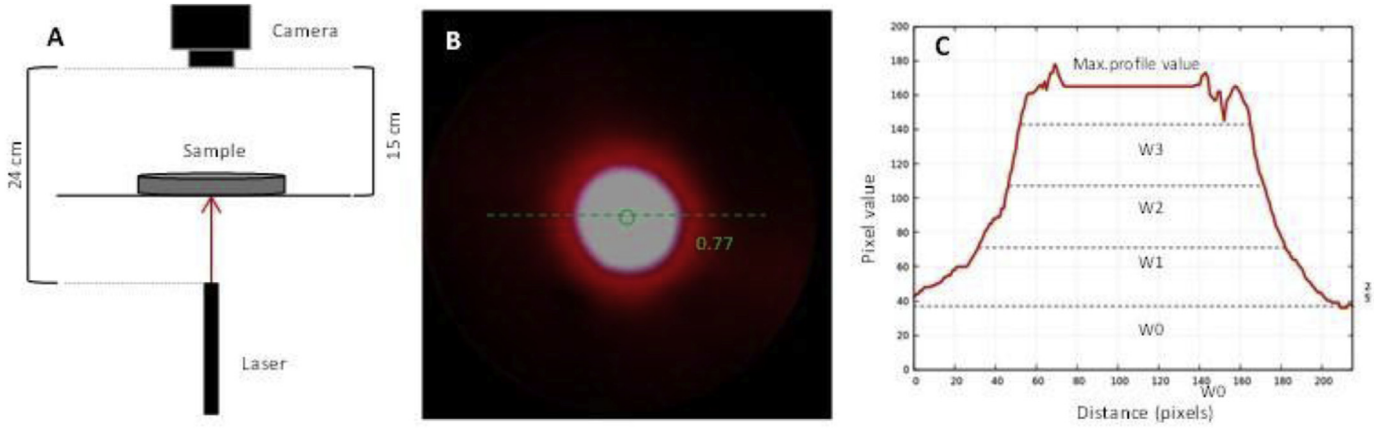

Fig. 2. A: Scheme of device setup (red arrow represents laser beam). B: The sample image obtained by the device (real image of light pattern generated onto cream surface). The green line crossing the laser pattern is located to compute the profile. C: Profile widths at the selected heights (w0, w1, w2 and w3: Profile widths (in pixels) at 20%, 40%, 60% and 80% of the maximum value). (For interpretation of the references to colour in this figure legend, the reader is referred to the Web version of this article.)

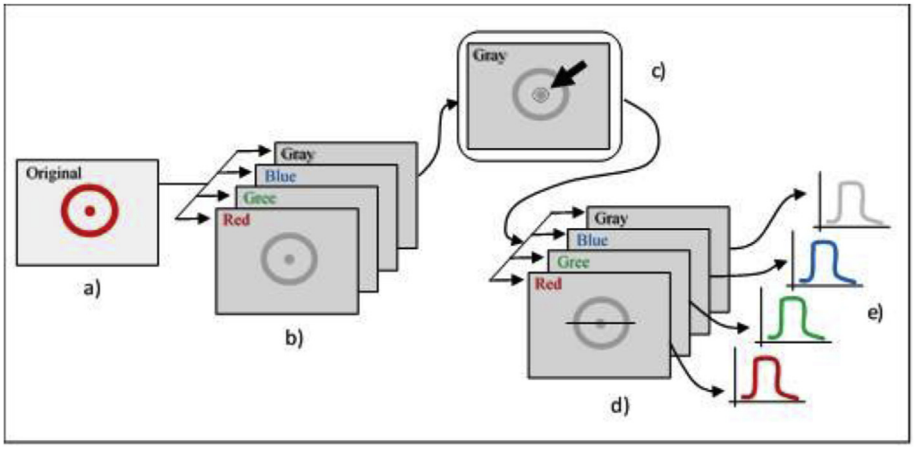

Fig. 3. Profile computation: Original image (a). Channel decomposition (b). Laser pattern blob detection (c). Profile lines selection (d). Profile extraction (e).

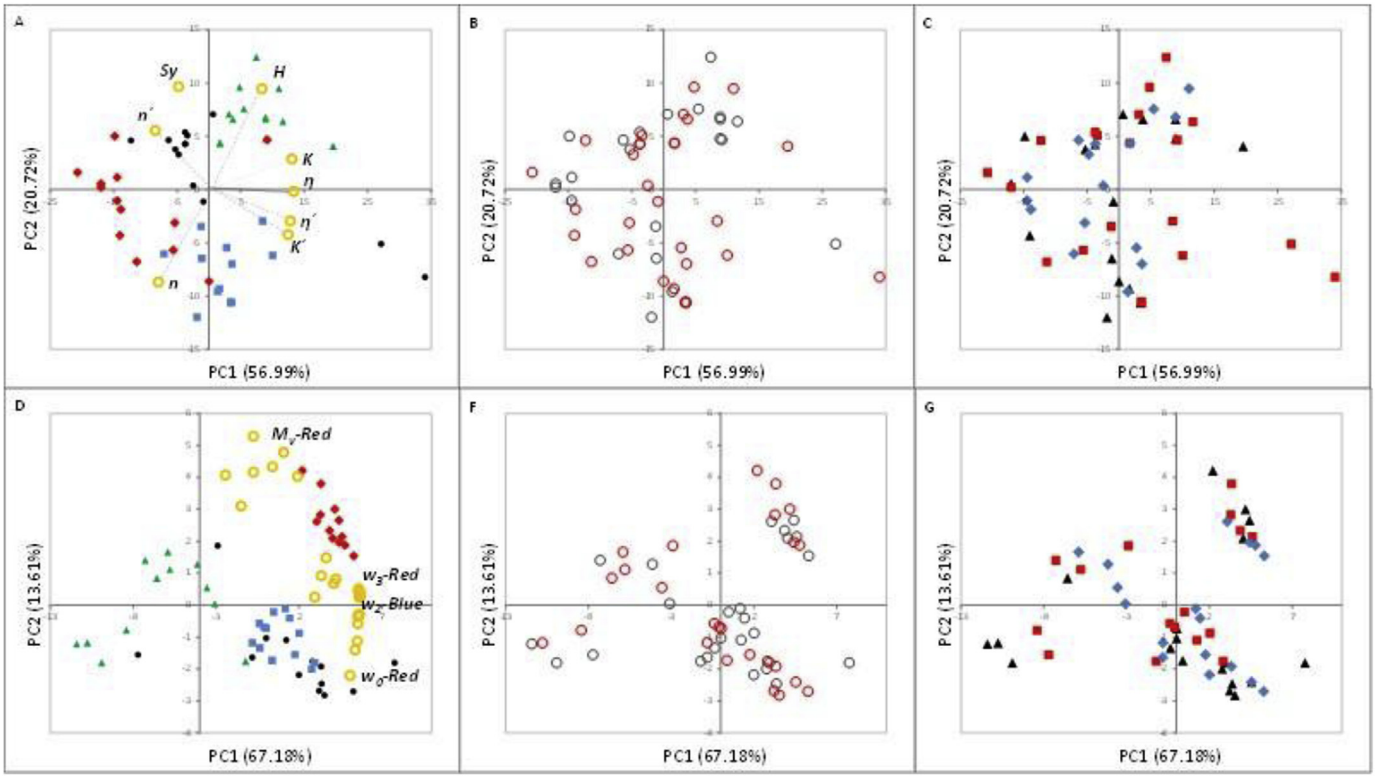

Fig. 4. Spaces of variance (PCAs) from the physico-chemical (top) and imaging (bottom) results. A and D (F1 labelling), B and D (F2 labelling) and C and E (F4 labelling). Yellow circumferences: descriptors (variables, only represented in A and D): ●: zucchini; ■: fish; ♦: chicken; ▲: spinach; ○: xhantan gum; ○: alginate; ▲: cooking robot; ♦: industrial mixer; ■: ultraturrax. (For interpretation of the references to colour in this figure legend, the reader is referred to the Web version of this article.)

material on moisture (X_w), fat (X_f), protein (X_p), fibre (X_{fi}) and total solutes (X_s) content. Moisture content was calculated based on the weight loss that the sample underwent when dried at a temperature between 130 °C and 133 °C. The Kjeldahl method was used to analyse protein content (AOAC 984.13 (A-D), 2006). Fat content was determined by the Soxhlet Extraction Method (AOAC 920.39). Total dietary fibre was measured by the McCleary Method (AOAC, 2009.01)[2−4].

2.4.4. Imaging device and data processing

2.4.4.1. Diffraction patterns capturing device. To obtain diffraction patterns, a device consisting in a red laser diode and a camera connected to a computer was built.

Fig. 2A shows the device setup. The laser beam was pointed through a Petri plate (55 mm ∅) containing 15 g of the cream sample (1 cm high). The distance between both was 9 cm. The distance between Petri plate and camera was 15 cm. An image of the scattered laser beam formed on the food surface and was captured by the camera (see 2A). The device was placed inside a black box to obtain uniform illumination. Temperature of capture was 20 °C.

The setup parameters and acquisition conditions were stablished taking into account the simplicity and reproducibility for a possible online job. The distances between elements, laser beam diameter, Petri plate diameter and thickness of sample were stablished based on the aim of obtaining a laser pattern with a correct distribution of colour zones, which allow us capturing a correct contrast in the images

(Fig. 2B). A high contrast and the colour zones well differentiated are essential in this technique to obtain correct colour profiles, from which the descriptors are generated (Fig. 2C). Both the laser diode (650 nm, 50 mW, 3 mm ∅) and the camera (HD cam Logitech C920) are low-cost components, and were connected to a conventional computer which ran Linux.

2.4.4.2. Image processing and extracting descriptors. Specific software was developed to automatically process and extract descriptors from images. As seen in Fig. 2B, a profile was obtained by selecting a line of the image crossing the laser pattern. The profile was obtained to represent the pixel intensity of each pixel of this line. This profile is a good representation of the laser pattern structure and several numerical descriptors can be derived from it.

The software performs two different tasks:

- Laser pattern detection, line selection and profile computation
- Profile analysis and descriptors extraction

2.4.4.2.1. Laser pattern detection, line selection and profile computation. An automatic algorithm was developed to detect the laser pattern and to compute its *centre of mass* (see Fig. 2B, green circumference). Once the *centre of mass* is detected, profile lines in any angle can be computed.

The algorithm works as follows (Fig. 3): captured images are RGB colour images. Every image is decomposed into four monochrome images (channels). Three of them represent the red, green and blue channels, and a fourth image is obtained from the grey conversion of the original image. The grey image is used to detect the laser pattern because it is obtained as a weighted mean of the other three.

To detect the laser pattern, an adaptive thresholding algorithm was employed to binarise the grey image to, thus, obtain a set of binary blobs. These blobs are located in the image by a labelling algorithm. The laser pattern is located as a circular blob near the centre of the image. Once detected, its *centre of mass* and *circularity* were computed. The centre of mass of a binary blob (c_x, c_y) was calculated as:

$$c_x = \frac{m_{01}}{m_{00}};\ c_y = \frac{m_{10}}{m_{00}}; \tag{3}$$

where m_{ij} are the moments of order $(i + j)$ defined as,

$$m_{ij} = \sum_x \sum_y x^i y^j f(x, y) \tag{4}$$

and $f(x,y)$ are the binary image values.

Circularity (φ) was computed as,

$$\varphi = \frac{area}{\pi . r^2} \tag{5}$$

where *area* is the blob area (in pixels) and *r* is the radius of the minimal circle that encloses the blob. A value far from 1.0 means that the blob is not circular, which thus indicates an error. Normally this is due to a laser pattern misdetection or to an image not being correctly captured. This value allows us to automatically detect problems in the process and prevents us from computing bad descriptors.

Once the centre of mass is computed, we can use it to select the lines crossing the laser pattern in the images and to compute its profiles.

2.4.4.2.2. Profile analysis and descriptors extraction. Given the wide captured variability in each image, it is worth analysing the profiles from the four channels because they provide different information. For each profile, several geometrical descriptors are computed to represent and simplify the profile data.

The set of profile descriptors computed for each cannel included: M_v: maximum profile value; *Area*: total profile area in pixels; w_0, w_1, w_2 *and* w_3: Profile widths (in pixels) at 20%, 40%, 60% and 80% of the maximum value (Fig. 2C); w_{30}: w_3/w_0 ratio; w_{31}: w_3/w_1 ratio.

The M_v and the *Area* provide information about the profile dimension. Values w_i contain information about the profile shape. They are calculated as the profile width at several heights (Fig. 2C). Finally, the w_{ij} descriptors provide more detailed information about the profile shape (profile slopes). Using this algorithm a set of 32 descriptors (8 descriptors per channel) is assigned to each captured image. If the confidence value (φ) goes below a certain threshold, the image is rejected or reviewed, which thus avoids bad captures being taken into account.

2.5. Statistical analysis

The rheological properties data were studied by a one-way variance study (ANOVA). In those cases with a significant effect (P-value < 0.05), the average was compared by Fisher's least significant difference (LSD). Analytical error (AE) and relative percentage of difference (RPD) were included to compare the results with the reference technique. A principal component analysis (PCA) was used to reduce the dimensionality of the rheological and image analysis data to perform a joint comparative analysis. A PCA is a multivariate unsupervised statistical method used to describe and reduce the dimensionality of a large set of quantitative variables to a small number of new variables, called principal components (PCs), which are the result of linear combinations of the original variables. Support Vector Machines (*SVM*) for regression (*SVM-R)* was applied to study the dependency between the rheological data and the image data by evaluating calibration (R^2), crossvalidation (R^2cv), prediction (R^2pred) coefficients and the root mean square errors (RMSE). Prediction procedures were followed using 60% of the samples as a training batch and 40% as a testing batch. *SVM* is a supervised learning methodology based on the statistical learning theory, which is commonly used for spectral data analyses (Boser et al., 1992). Procedures were performed with PLS Toolbox, 6.3 (Eigenvector Research Inc., Wenatchee, Washington, USA), a toolbox extension in the Matlab 7.6 computational environment (The Mathworks, Natick, Massachusetts, USA).

3. Results and discussion

3.1. Physico-chemical characterisation

The proximal composition of creams according to raw materials is collected in Table 1. The results showed the highest statistically difference was in fibre fraction (X_{fi}), with the amount of zucchini and spinach doubling that of chicken and fish. The rest of the parameters also presented some statistical differences, although similar values with around a 3% difference as a maximum (e.g X_p and X_w). The variance of the physico-chemical descriptors was analysed to know the role of each

Table 1
Proximal composition of the produced creams according to F1 (raw material).

Raw material	*Xp*	*Xf*	*Xfi*	*Xw*	*Xs*
Zucchini	0.015 ± 0.001b	0.020 ± 0.005b	0.012 ± 0.002b	0.89 ± 0.03a	0.11 ± 0.01a
Fish	0.011 ± 0.002a	0.017 ± 0.003a	0.007 ± 0.002a	0.871 ± 0.01a	0.129 ± 0.02b
Chicken	0.015 ± 0.001b	0.018 ± 0.005 ab	0.007 ± 0.001a	0.869 ± 0.01a	0.131 ± 0.01 ab
Spinach	0.012 ± 0.001a	0.017 ± 0.002a	0.012 ± 0.002b	0.888 ± 0.02a	0.112 ± 0.01a

Xp: protein content, Xf: fat content, Xfi: fibre content, Xw: moisture content, Xs: total solutes content. Letters within columns mean significant differences at $\alpha \leq 0.05$.

Table 2
Results of the main effect significance for each factor.

Factors	K	n	η	K'	n'	η'	H	Sy
F1	**99.53/0.0001**	**37.16/0.0001**	**98.09/0.0001**	28/0.0001	4.09/0.01	**75.7/0.0001**	**204.23/0.0001**	**216.1/0.0001**
F2	15.33/0.0001	12.39/0.001	14.6/0.004	31.81/0.0001	**163.93/0.0001**	16.30/0.0001	25.12/0.0001	151.2/0.0001
F3	81.88/0.0001	0.16/0.69	56.91/0.0001	**95.79/0.0001**	8.64/0.005	55.56/0.0001	33.09/0.0001	116.3/0.0001
F4	22.9/0.0001	3.49/0.038	4.22/0.02	13.6/0.0001	4.52/0.015	5.15/0.009	32.25/0.0001	2.08/0.13

The results express F-ratio/p-value. F1: raw material; F2: biopolymer; F3 biopolymer concentration; F4: homogenisation system; *K:* consistence index; n: flux behaviour index; *η:* apparent viscosity, H: hysteresis area; Sy: syneresis. Symbols with ´ mean the same parameter from the second sweep (*K′, n´* and *η′*) and the hysteresis area (*H*). Bold numbers mean the maximum value for the F-ratio within each column.

Table 3
Modelling results for single physico-chemical descriptors and the physico-chemical space of variance from the imaging data.

Modelling parameter	K	n	η	K'	n'	η'	H	Sy	PC1	PC2
$RMSE_{Cal}$	1.07	0.01	120	0.84	0.01	87	546.0	1.38	0.99	0.48
$RMSE_{CV}$	1.8	0.01	161.5	1.44	0.01	123	628.5	3.88	1.72	1.51
$RMSE_{Pred}$	1.71	0.01	111	1.14	0.01	79	552.9	2.96	1.78	1.29
$Bias_{Cal}$	0.01	0.01	−20.58	0.01	0.01	−10.70	−188.6	0.04	−0.05	0.01
$Bias_{CV}$	0.03	0.01	−31.72	−0.12	0.01	−18.80	−208.6	−0.25	0.04	0.02
$Bias_{Pred}$	−0.21	0.01	−19.15	−0.1	0.01	−8.9	−188.7	0.06	−0.31	−0.05
R^2_{Cal}	0.98	0.96	0.81	0.98	0.88	0.85	0.81	0.98	0.99	0.99
R^2_{CV}	0.93	0.92	0.59	0.9	0.81	0.68	0.73	0.88	0.96	0.95
R^2_{Pred}	0.97	0.94	0.83	0.96	0.81	0.87	0.8	0.94	0.97	0.96
AE	0.95	0.02	24.6	0.18	14.00	6.82	18.1	0.21	0.33	0.21
SD	2.15	0.01	47.2	1.03	0.01	43.0	210.8	1.10	0.95	0.82
RPD	0.09	0.18	3.3	0.79	3.28	1.63	3.06	0.09	0.97	0.59

K: consistence index, n: flux behaviour index and η: apparent viscosity at $100s^{-1}$ from the first sweep; the same from the second sweep K', n' and η'; H: hysteresis area; Sy: syneresis. PC1and PC2: principal components 1 and 2 from the physico-chemical space of variance (Figure X–A). RMSE: root mean square error; Bias: differences in expected value; Cal: calibration; CV: cross-validation; Pred: prediction; AE: analytical error; SD_{FQ}: standard deviation of the physicochemical properties; RPD: relative percentage difference.

Table 4
Glossary of terms, symbols and abbreviations.

Symbol		Symbol	
F1	raw material	Φ	circularity
F2	biopolymer concentration	M_v	maximum profile value
F3	biopolymer type	*w0*	20% Profile width
F4	homogenisation system	*w1*	40% Profile width
w.b	wet basis	*w2*	60% Profile width
σ	shear stress	*w3*	80% Profile width
γ	shear rate	w_{30}	w3/w0
H	histeresys area	w_{31}	w3/w1
K	consistence index	*PCA*	principal component analysis
n	flux behaviour index	*PCs*	principal components
η	apparent viscosity	*SVM-R*	Support Vector Machines
S_y	syneresis	R^2	calibration coefficient
X_w	water fraction	R^2cv	crossvalidation coefficient
X_f	fat fraction	R^2pred	prediction coefficient
X_p	protein fraction	*RMSE*	root mean square errors
X_{fi}	fibre fraction	*AE*	analytical error
X_s	solutes fraction	*RPD*	relative percentage difference
RGB	red, green, blue	*BIAS*	differences in expected value
C	centre of mass		

factor and to determine the significance of their main effects. The F-ratio and its p-value from each factor and per descriptor were calculated and are found in Table 2. The p-values showed significance for all the main effects on all the physico-chemical descriptors, except F3 for n' and F4 for S_y. F1 (raw material) generally presented the maximum F-ratio values, followed by F3 (concentration) in most of cases. With n, K'and Sy, F2 was the second highest. The raw results of the physico-chemical analyses can be consulted in Table 4 (Supplementary Material).

However, to improve the understooding and visualisation of that variance space, a PCA was done with all the physico-chemical descriptors. This procedure allowed the reduction of dimensionality and the analysis of the total variance in the experiment simultaneously. Fig. 4A shows the biplot of the generated PCA space, where the average scores from each cream category and the loadings from each physico-chemical descriptor are represented. Two PCs, which are linear combinations of the original variables, delimited this space of physico-chemical variance. PC1 collected 56.99% of variance, with 20.72% for PC2. Samples were placed in different zones of the space, but the clustering following raw material (F1) was maintained. The four raw materials were differentiable from the physico-chemical descriptors with different intensities. Each raw material displayed wide variance, which was induced by the other factors. In some cases, samples were placed inside another cluster because of their high level of modification. The zucchini creams appeared in a high relationship with Sy, H and n', but two samples appeared in a high relationship with K, K',η and η'. These creams were those with 0.6% of biopolymers and turrax. Spinach also showed a high loading with Sy, n'and H, but also with K, K', η and η'. This means that high viscosity and consistence were induced because of spinach properties compared to zucchini. With chicken, the properties were similar to zucchini, but trended to high n values, and inversely with H. The fish creams presented a higher loading of n, K', and η' than chicken. Overall, animal tissues appeared to increase the stability of creams by reducing Sy and H, and having high values for K', and η'. When the PCA was studied according to the other production variables, F2 (biopolymer, Fig. 4B), F3 (biopolymer concentration) or F4 (homogenisation system, Fig. 4C), no clustering pattern was observed according to the multifactor ANOVA results (Table 2). So we concluded that the variance generated by F2, F3 and F4 depended on F1.

3.2. Imaging characterisation

To make a comparison with the physico-chemical results, the imaging data exploration was done directly by PCA due to the high

dimensionality of the generated image information. Fig. 4D shows the PCA, space of image variance, which was delimited by PC1 and PC2, having collected 67.18% and 13.61% of the total image data variance, respectively. In this case, the spontaneous clustering based on F1 was also observed, although the relative places of raw materials showed differences in this case. The zucchini and fish creams were close to one another, although the zucchini creams once again maintained the samples with 0.6% biopolymers and turrax placed away from the nucleus of their raw material cluster. Spinach and chicken appeared to be quite isolated from the rest, although one spinach cream category was placed with the fish creams and the non-modified chicken sample within the zucchini cluster. Thus the effect of factors seemed to be the same for this block of descriptors. When PCA space was labelled according to F2, F3 or F4 (Fig. 4E and F), the results were according to the physico-chemical PCA. No clustering based on biopolymer type or homogenisation system was observed.

Most of the image descriptors presented high loadings in PC1. Some of the most important ones were w_2 and w_3 from all the image channels, which implies a high colinearity. This colinearity can be explained by these descriptors having an equivalent response to the modifications to shape the laser pattern due to differences in the optical properties of the cream matrix. Moreover, PC2 gave a high explanation level for the variability of the chicken creams, where the main descriptors were the maximum profile values for all the channels, with w_{30} and w_{31} for R and the grey images. These descriptors revealed modifying profile slopes for this cream cluster.

The observed results proved the sensitivity of the selected image descriptors with the variability of the creams due to processing. In the same way as the physico-chemical descriptors, a space of variability was described, where F1 was the factor with the strongest impact on sample distribution. The fact that both data blocks showed an equivalent PCA behaviour under the same conditions could not mean either correlation or causality because the placing of samples showed differences in the respective PCA distributions. In fact the generated changes in the physico-chemical properties might not have any equivalence with the laser patterns. However, after exploring the single relationships between both blocks of descriptors, modelling tendencies were observed. Fig. 5 provides an example of two rheological descriptors (*K* and *n*) *vs.* descriptor w_3 from the red channel (one of the most important descriptors in PC1 of the space of image variance; PCA). We can observe a covariation of *w_3-red* with these rheological descriptors. Across the generated model, samples were also grouped following the raw materials: spinach was placed on the maximum extreme for K, but on the minimum for n and w_3-red. The chicken creams were placed on the inverse extreme, while the most of the zucchini and fish creams were placed around the central zone. The observed model showed the inverse relationship between consistence (K) and w_3. This means that when consistence increased, laser pattern profile width narrowed, and then less light was transmitted across the cream matrix. This effect proved the dependence of the light-matrix interaction on the resulting signal due to the differences in the proximal composition of each raw material. Some studies agree with this observation: Udomkun et al. (2014) and Romano et al. (2011) have reported that the evolution of moisture and solutes in a vegetal matrix (apple, papaya, etc.) during drying processes brings about changes in this type of laser patterns, which correlate with measured moisture, sugars and other solutes. Apart from the chemical composition, vegetal matrices have also been characterised by laser backscattering imaging in terms of mechanical properties by Mollazade et al. (2013). Moreover, those phenomena have also been applied to processed muscular tissues, concretely Fulladosa et al. (2017) reported the capability of this technique to detect changes due to drying and proteolysis on dry-cured hams.

In the case of the cream samples, moisture (X_w) and the solutes fraction (X_s) are similar. The main differences between creams were seen for fibre fraction (X_{fi}). Although proteins and lipids were similar, their chemical nature could also modify image descriptors.

Thus by taking into account the observed results and the complexity of the studied food matrix herein, various sources of laser patterns variance were suggested following studies by other authors and their conclusions. The main source was the effect of solid particles from a physical point of view. Each raw material provided solid particles with different sizes and compositions (e.g., cellulose, starch, muscular fibres, etc.) that influenced the diffractive properties of the matrix (Nicolaï et al., 2007). Moreover, the solubilised components from each raw material also generated variability because of the influences on the refractive properties of liquid phase (e.g., myoglobin, chlorophyll, peptides, vitamins, polyphenols, sugars, soluble fibres, minerals, etc.). From a chemical point of view, and for both the solid particles and solubilised compounds, the plausible presence of chemical bonds absorbing part of radiation gave rise firstly to modifications to transmittance, and then to the generated laser patterns (Mireei et al., 2010). This could explain why the spinach creams had the lowest w_3-red (Fig. 5). The reason for this is because spinach contains large amounts of chlorophyll, which has an absorption peak at around 650 nm, which is precisely the wavelength of the laser used in this experiment (Tamburini et al., 2015). This effect was also reported by Romano et al. (2012). In that study, the moisture of red, yellow and green peppers were predicted using laser backscattering, however weak correlations were obtained for the green samples when 650 nm was used due to the influence of strong absorption band of chlorophyll. The presence of biopolymers also led to alterations being made to the optical properties by themselves, such as the refractive index and increasing opacity (Basavaraju et al., 2007). All the above-mentioned effects can be modified because of the homogenisation process. This process reduces particle size and makes dispersions more homogeneous, which thus influences the light-matrix interaction.

Overall, the crossing effects of the four selected factors made it difficult to explain the observed results of a variance space of production using descriptor by descriptor from the image data block. However following the results of other authors, it seems that it might adequately used as a multivariate database to model the behaviour of creams.

3.3. Modelling the defined space of variance

The relationship between the physico-chemical descriptors and image descriptors was studied by modelling with SVM. These studies were performed by correlating the image descriptors data matrix with each physico-chemical descriptor singly and with the PC1 and PC2 scores from the space of physico-chemical variance (Fig. 4A), which simultaneously represent the physico-chemical behaviour of the samples. This approach allowed us to determine if the image data could predict the place of produced cream categories in this generated space of physico-chemical variance.

Table 3 shows the results of the modelling parameters. Overall, the coefficients of calibration, cross-validation and prediction came close to 1, be it with differences between parameters. The maximum prediction coefficients regarding single parameters went to K (0.97), K' (0.96), n (0.94) and Sy (0.94). These parameters also presented high fit values for both calibration and cross-validation. Moreover, there were parameters with lower coefficients, such as η (0.83), η' (0.87), n' (0.81) and H (0.80). The prediction of these parameters was more difficult than the first ones, but no coefficient was lower than 0.8. These results were in accordance with the observed analytical error (AE), where those parameters with reduced prediction coefficients also had higher error compared to the observed values. When those results were expressed as the relative percentage difference (RPD) the maximum relative difference was 3.28% for η and n', while K and Sy the minimum ones around 0.09%. Thus the technique did not predict with 0% of error, however the results seemed satisfactory enough to characterise those studied physicochemical properties at experimental conditions. Moreover, when standard deviation of physicochemical data was observed, the highest values were also for parameters with lowest coefficients. That

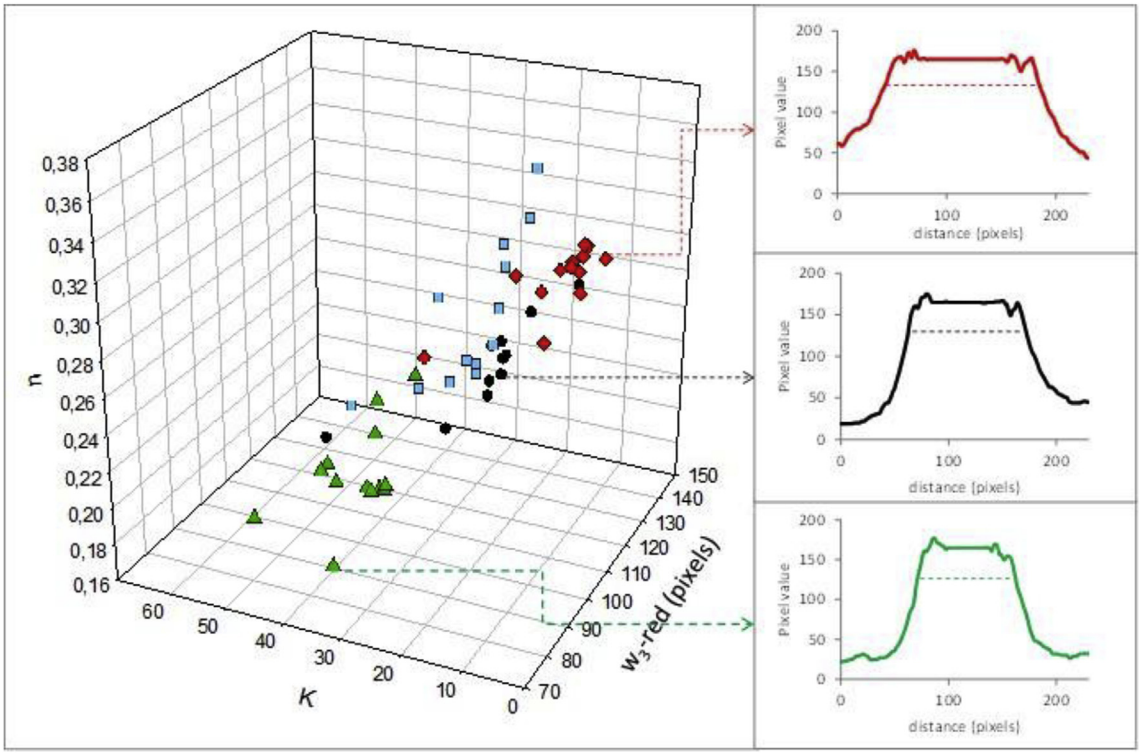

Fig. 5. Relationship between rheological descriptors consistence index (*K*) and flux behaviour index (*n*) with image descriptor *w3-red* (80% profile width from red channel) from all the creams. Plots are examples of laser-pattern profiles from the red image channels, where w_3 is indicated by a dotted line. ●: zucchini; ■: fish; ♦: chicken; ▲: spinach. (For interpretation of the references to colour in this figure legend, the reader is referred to the Web version of this article.)

fact could mean that the observed error could be influenced not only by analytical error of the technique but also by the heterogeneity of samples at rheological analytics.

This behaviour was in accordance with the covariation observed in Fig. 5 which, in this case, could be improved because of the combination of all the image descriptors. This covariation allowed the modelling of the physico-chemical descriptors using the image data, be it with different accuracy levels. Other authors have also reported different accuracy levels in modelling coefficients for several physico-chemical properties of food matrices using this technique. Some of them are quality control properties in tomato fruit (Tu et al., 2000), quality control properties and presence of seeds in watermelon (Mohd Ali, Hashim, Bejo and Shamsudin, 2017a, 2017b), quantifying chilling damage in bananas (Hashim et al., 2013), etc. This means that the technique is useful for these purposes. However, the noise generated in the signal differently affects the single prediction of each parameter. Thus the modification of some elements in a given device configuration would probably reduce the signal noise and optimise the results for individual physico-chemical parameters predictions.

In PC1 and PC2 modelling, the prediction coefficients were 0.97 and 0.96, respectively. The calibration, cross-validation and prediction parameters were successful, and showed that the technique was capable of correctly placing the samples in the space of physico-chemical variance. This result indicates that, despite some physico-chemical descriptors presenting less modelling coefficients individually, their variances were better predicted when they were all combined linearly to generate PCs. This effect could be explained because, in this case, the variance of the laser patterns did not depend on only one factor. The combination of factors generated common rheological behaviours among the cream categories for a given parameter, but it was not parallel for the laser patterns, which presented different image information for each category. Thus the laser pattern was unable to display good dependency on an individual physico-chemical parameter, rather with the combinational response of them all, such as PC1 and PC2, which collected most of the variance from the physico-chemical descriptors at the time like a "physico-chemical fingerprint".

When the predicted PC1 and PC2 data were included in the space of physico-chemical variance, we observed how samples from the test batch were placed around the correct coordinates (Fig. 6). This shows how the observed relationship between the physico-chemical and image information can be used to characterise creams quite accurately. Thus the physico-chemical properties of a cream from this production space can be controlled by the proposed image descriptors, and by placing the

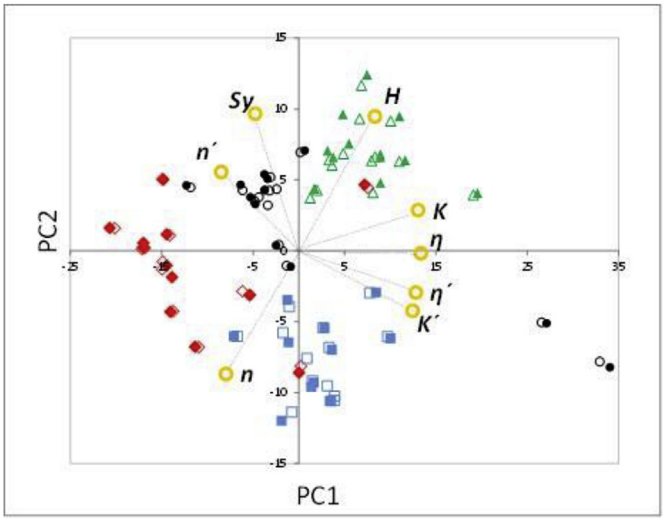

Fig. 6. The observed (physico-chemical) and predicted (by the image technique) PC1 and PC2 coordinate in the physico-chemical space of variance. Values represent the average of each cream category. Points are labelled based on F1 (raw materials) ●: zucchini; ■: fish; ♦: chicken; ▲: spinach. Empty symbols indicate the average predicted values.

output PCs coordinates into the pre-stablished space of variance. The recognition capacity of this technique could thus be useful as a quality control application at a production plant where many products are produced at one time. Thus being able to know whether a given cream category batch was produced with correct physico-chemical properties in a short time with the appropriate technical requirements is plausible. In addition, new formulae with similar physico-chemical features can be included in the model to increase captured variability and to improve the learning process and the accuracy of a given quality control.

4. Conclusions

The proposed technique was capable of collecting the variance generated in creams because of the effect of the raw material, biopolymers and homogenisation system according to the laser-patterns modifications, which were defined by the developed image descriptors system. The prediction models obtained between the image descriptors and the physico-chemical properties of creams were able to characterise different samples in a non-destructive and rapid way. It seems that this new technique contains new possibilities in applications focused on fluid foods, which could obtain rapid information from a high amount of samples in a reduced time.

References

Adebayo, S.E., Hashim, N., Abdan, K., Hanafi, M., 2016. Application and potential of backscattering imaging techniques in agricultural and food processing - a review. J. Food Eng. 169, 155–164. http://doi.org/10.1016/j.jfoodeng.2015.08.006. Arendse, E., Fawole, O.A., Magwaza, L.S., Opara, U.L., January 2018. Non-destructive prediction of internal and external quality attributes of fruit with thick rind: a review. J. Food Eng. 217, 11–23. http://doi.org/10.1016/j.jfoodeng.2017.08.009.

Barbin, D.F., Kaminishikawahara, C.M., Soares, A.L., Mizubuti, I.Y., Grespan, M., Shimokomaki, M., Hirooka, E.Y., 2015. Prediction of chicken quality attributes by near infrared spectroscopy. Food Chem. 168, 554–560. http://doi.org/10.1016/j.foodchem.2014.07.101.

Basavaraju, K.C., Demappa, T., Rai, S.K., 2007. Miscibility studies of polysaccharide Xanthan gum and PEO (polyethylene oxide) in dilute solution. Carbohydr. Polym. 69 (3), 462–466. http://doi.org/10.1016/j.carbpol.2007.01.004.

Boser, E., Vapnik, N., Guyon, I.M., Laboratories, T.B., 1992. Training algorithm margin for optimal classifiers. Perception 144–152.

de Prados, M., Fulladosa, E., Gou, P., Muñoz, I., Garcia-Perez, J.V., Benedito, J., 2015. Non-destructive determination of fat content in green hams using ultrasound and X-rays. Meat Sci. 104C, 37–43. http://doi.org/10.1016/j.meatsci.2015.01.015.

Fuentes, E., Alcañiz, M., Contat, L., Baldeón, E.O., Barat, J.M., Grau, R., 2017. Influence of potential pulses amplitude sequence in a voltammetric electronic tongue (VET) applied to assess antioxidant capacity in aliso. Food Chem. 224, 233–241. http://doi.org/10.1016/j.foodchem.2016.12.076.

Fulladosa, E., Rubio-Celorio, M., Skytte, J.L., Muñoz, I., Picouet, P., 2017. Laser-light backscattering response to water content and proteolysis in dry-cured ham. Food Contr. 77, 235–242. http://doi.org/10.1016/j.foodcont.2017.02.001.

Hashim, N., Pflanz, M., Regen, C., Janius, R.B., Abdul Rahman, R., Osman, A., et al., 2013. An approach for monitoring the chilling injury appearance in bananas by means of backscattering imaging. J. Food Eng. 116 (1), 28–36. http://doi.org/10.1016/j.jfoodeng.2012.11.018.

IDDSI, 2016. International Dysphagia Diet Standardization Initiative. www.iddsi.org, Accessed date: 16 February 2016.

Mireei, S.A., Mohtasebi, S.S., Massudi, R., Rafiee, S., Arabanian, A.S., 2010. Feasibility of near infrared spectroscopy for analysis of date fruits. Int. Agrophys. 24 (4), 351–356. Retrieved from https://www.scopus.com/inward/record.uri?eid=2-s2.0-79955023784&partnerID=40&md5=bda54a95925b007416fe8354a2214b79.

Mizrahi, S., 2010. Syneresis in food gels and its implications for food quality. In: Chemical Deterioration and Physical Instability of Food and Beverages (pp. 324–348), . http://doi.org/10.1533/9781845699260.2.324.

Mohd Ali, M., Hashim, N., Bejo, S.K., Shamsudin, R., 2017a. Laser-induced backscattering imaging for classification of seeded and seedless watermelons. Comput. Electron. Agric. 140, 311–316. http://doi.org/10.1016/j.compag.2017.06.010.

Mohd Ali, M., Hashim, N., Bejo, S.K., Shamsudin, R., 2017b. Quality evaluation of watermelon using laser-induced backscattering imaging during storage. Postharvest Biol. Technol. 123, 51–59. http://doi.org/10.1016/j.postharvbio.2016.08.010.

Mollazade, K., Omid, M., Tab, F.A., Mohtasebi, S.S., 2012. Principles and applications of light backscattering imaging in quality evaluation of agro-food products: a review. Food Bioprocess Technol. 5 (5), 1465–1485. http://doi.org/10.1007/s11947-012-0821-x.

Mollazade, K., Omid, M., Akhlaghian Tab, F., Kalaj, Y.R., Mohtasebi, S.S., Zude, M., 2013. Analysis of texture-based features for predicting mechanical properties of horticultural products by laser light backscattering imaging. Comput. Electron. Agric. 98, 34–45. http://doi.org/10.1016/j.compag.2013.07.011.

Nicolaï, B.M., Beullens, K., Bobelyn, E., Peirs, A., Saeys, W., Theron, K.I., Lammertyn, J., 2007. Nondestructive measurement of fruit and vegetable quality by means of NIR spectroscopy: a review. Postharvest Biol. Technol. 46 (2), 99–118. http://doi.org/10.1016/j.postharvbio.2007.06.024.

Romano, G., Nagle, M., Argyropoulos, D., Müller, J., 2011. Laser light backscattering to monitor moisture content, soluble solid content and hardness of apple tissue during drying. J. Food Eng. 104 (4), 657–662. http://doi.org/10.1016/j.jfoodeng.2011.01.026.

Romano, G., Argyropoulos, D., Nagle, M., Khan, M.T., Müller, J., 2012. Combination of digital images and laser light to predict moisture content and color of bell pepper simultaneously during drying. J. Food Eng. 109 (3), 438–448. http://doi.org/10.1016/j.jfoodeng.2011.10.037.

Tamburini, E., Ferrari, G., Marchetti, M.G., Pedrini, P., Ferro, S., 2015. Development of FT-NIR models for the simultaneous estimation of chlorophyll and nitrogen content in fresh apple (Malus Domestica) leaves. Sensors (Switzerland) 15 (2), 2662–2679. http://doi.org/10.3390/s150202662.

Tu, K., Jancsók, P., Nicolaï, B., De Baerdemaeker, J., 2000. Use of laser-scattering imaging to study tomato-fruit quality in relation to acoustic and compression measurements. Int. J. Food Sci. Technol. 35 (5), 503–510. http://doi.org/10.1046/j.1365-2621.2000.00407.x.

Udomkun, P., Nagle, M., Mahayothee, B., Müller, J., 2014. Laser-based imaging system for non-invasive monitoring of quality changes of papaya during drying. Food Contr. 42, 225–233. http://doi.org/10.1016/j.foodcont.2014.02.010.

Verdú, S., Vásquez, F., Ivorra, E., Sánchez, A.J., Barat, J.M., Grau, R., 2017. Hyperspectral image control of the heat-treatment process of oat flour to model composite bread properties. J. Food Eng. 192, 45–52. http://doi.org/10.1016/j.jfoodeng.2016.07.017.